ELUCIDATION OF NITRATE REDUCTION MECHANISMS ON A
PD/IN BIMETALLIC CATALYST USING ISOTOPE LABELED
NITROGEN SPECIES

BY

RUI ZHANG

THESIS

Submitted in partial fulfillment of the requirements
for the degree of Master of Science in Environmental Engineering in Civil Engineering
in the Graduate College of the
University of Illinois at Urbana-Champaign, 2011

Urbana, Illinois

Advisers:

      Professor Charles J. Werth
      Associate Professor Timothy J. Strathmann

ABSTRACT

Catalytic hydrogenation over Pd-based catalysts has emerged as an effective treatment approach for nitrate (NO_3^-) removal, but its full-scale application for direct treatment of drinking water or ion exchange regenerant brines requires improved selectivity for the end-product dinitrogen (N_2) over toxic ammonia species (NH_4^+, NH_3). A key to improving N_2 versus NH_4^+ production is to elucidate nitrate reduction pathways and identify the key intermediate(s) that determine selectivity. To address this challenge, aqueous reduction experiments with an Al_2O_3-supported Pd/In bimetallic catalyst were conducted using isotope-labeled nitrite ($^{15}NO_2^-$), the first reduction intermediate of NO_3^-, alone and in combination with unlabeled proposed reduction intermediates (N_2O, NO), and using N_2O and NO alone, each as a starting reactant. Use of ^{15}N-labeled species eliminated interference from ambient $^{14}N_2$ when assessing mass balances and product distributions. Simultaneous catalytic reduction of $^{15}NO_2^-$ and $^{14}N_2O$ showed no isotope mixing in the final N_2 product, demonstrating that N_2O does not react with other NO_2^- reduction intermediates. N_2O reduction alone also yielded only N_2, verifying that N_2O reduction occurs after the reaction step controlling final N_2/NH_4^+ product distribution. In contrast, simultaneous catalytic reduction of $^{15}NO_2^-$ and ^{14}NO yielded mixed-labeled N_2 (mass 29), and ^{15}NO reduction alone yielded both N_2 and NH_4^+, indicating that NO is a key intermediate involved in determining final product selectivity. N_2/NH_4^+ product selectivity was also evaluated as a function of varying initial ^{15}NO concentration, and results show that selectivity for N_2 increases with initial NO concentration to a point, above which product selectivity remains unchanged. This trend is attributed to the increasing importance of N-N pairing reactions leading to N_2O formation as the concentration of catalyst-adsorbed NO (NO_{ads}) increases to a point of saturating available adsorption sites, above which no further increases in N_2 selectivity occur. These results are important because they yield mechanistic insights into the NO_3^- reduction pathway and information on how catalytic reduction processes can be optimized to maximize N_2 production over NH_4^+.

ACKNOWLEDGEMENTS

TABLE OF CONTENTS

LIST OF FIGURES

LIST OF TABLES

CHAPTER 1: INTRODUCTON

Nitrate (NO_3^-) is a common contaminant detected in surface water and underground aquifers. It can result from overuse of agricultural fertilizers, sewage discharges, and contaminant leachate from landfills [1]. Nitrate contamination can cause serious health risks to humans, such as methemoglobinemia (blue baby syndrome) and cancer [2]. The latter risk results when NO_3^- reduction intermediates (e.g., nitrite) are converted to nitroso compounds in the human body [3]. Although the concentration of NO_3^- in the natural environment is generally less than 2 mg/L, domestic groundwater wells and other impacted water sources are often found with concentrations exceeding the maximum contaminant level [3] of 10 mg/L NO_3^- N (44 mg/L as NO_3^-). Epidemiological studies have linked exposure to NO_3^- at concentrations well below Environmental Protection Agency (EPA) and World Health Organization (WHO) standards to several cancers and negative birth outcomes [4]. Numerous technologies exist for removing nitrate from drinking water. A key challenge is developing more sustainable technologies that remove nitrate from drinking water and do not create unwanted byproducts.

Conventional methods for NO_3^- treatment can be divided into two categories, physicochemical and biological. Physicochemical treatment methods, such as ion exchange, electrodialysis, and reverse osmosis, are effective, but only serve to transfer NO_3^- from water into a concentrate phase which requires further treatment or disposal [5,6,7,8]. Biological denitrification is commonly used for wastewater treatment, but less so for drinking water due to challenges associated with the variability of incoming water quality and operational control, the production of unwanted side products, high turbidity in finished water, and concerns for pathogen exposure [9,10,11]. Catalytic hydrogenation with Pd-based bimetallic catalysts has emerged as a promising new technology for treating NO_3^- and other oxyanions (e.g., nitrite, bromate, perchlorate) in drinking water or concentrate waste streams that is capable of

converting NO_3^- to harmless dinitrogen gas (N_2) [12,13,14,15].

Rapid nitrate reduction has been reported for supported Pd/Cu, Pd/In, and Pd/Sn catalysts using exogenous hydrogen (H_2) as the reducing agent [16,17,18,19,20]. A proposed but heretofore unproven reduction pathway is shown in **Scheme 1**. Nitrite (NO_2^-), nitric oxide (NO), and nitrous oxide (N_2O) are reduced on monometallic Pd [21,22,23], but a second metal (e.g., Cu, In, Sn, Co) is needed as a promoter for the first reduction step converting NO_3^- to NO_2^- [21,24]. It has been proposed that NO_3^- adsorbs onto the bimetallic ensemble and is reduced to NO_2^-, which is further converted to other N-containing intermediates on Pd. The stable end-products of catalytic nitrate reduction are dinitrogen (N_2) and ammonium (NH_4^+); the former is innocuous and ubiquitous in the atmosphere, while the latter is considered a hazardous aquatic pollutant. Hence, catalysts and operating conditions that select for N_2 production are desirable.

A number of factors have been reported to affect the N_2/NH_4^+ end-product distribution during aqueous NO_3^- or NO_2^- reduction on Pd-based catalysts. These include pH, temperature, N:H molar ratios, Pd nanocluster size and shape, and catalyst support [25,26,27,28,29]. A fundamental issue that affects the impact of all such factors on selectivity is the NO_3^- reduction pathway. More specifically, what key intermediate(s) control the end-product distribution? Reduction of NO_2^- has been identified as a key step in the overall NO_3^- reduction pathway that determines selectivity [30,31,32,33]. In a recent FTIR-based study, Ebbesen *et al* (2008) [34] reported detecting formation of absorbed NO (NO_{ads}) from aqueous NO_2^- on a Pd/Al_2O_3 catalyst in the presence of H_2. Because no change in $NH_{2(ads)}$ or NH_4^+ was detected for the first 12 min during the hydrogenation of NO_{ads}, they postulated that NO_{ads} does not contribute to NH_4^+ production during NO_2^- reduction [34]. However, in a follow-up study they reported that NH_4^+ instead of N_2 was formed predominantly from NO_{ads} during NO_2^- reduction over Pt/Al_2O_3 [35].

NO has also been proposed as a key intermediate that determines selectivity for N_2 and NH_4^+ as indicated in **Scheme 1** [20,36]; however, there is no direct experimental evidence to support this in aqueous systems. In gas phase systems, both N_2 and NH_3 were observed as NO reduction products on three-way catalysts [37,38,39]. In contrast to NO, N_2O is a known intermediate that has been measured during NO_3^- reduction [20,35]. It has been proposed as the direct precursor to N_2. Conflicting reports concerning the role of NO_2^- and NO on final product selectivity highlight the need for further elucidation of the NO_3^- reduction pathway.

The goals of this work are to elucidate the NO_3^- reduction pathway(s) on a Pd/In bimetallic catalyst supported on γ-Al_2O_3 that was previously shown to exhibit high activity for NO_3^- reduction and regenerability after sulfide fouling [15,17,40,41]. Specifically, experiments were conducted to identify the key intermediates that determine selectivity for N_2 versus NH_4^+, and to assess how changes in concentrations of intermediate species affect the preference of pathways leading to each stable end-product. To accomplish this, ^{15}N-labeled nitrogen species were used to aid in tracking nitrogen mass balances through the reduction process. Kinetics experiments used NO_2^- as the initial reactant, since it has been unambiguously identified as the first intermediate in the nitrate reduction pathway [24]. Selectivity was measured using [15]NO_2^- alone, and in the presence of unlabeled NO and N_2O. In the latter experiment, the mix of N isotopes in N_2 is used to determine which species are involved in N-N pairing reactions necessary to form N_2. Product selectivity experiments were also conducted using NO and N_2O as initial reactants. Initial concentrations of NO_2^- and NO were varied to evaluate the effects of NO_{ads} concentration on selectivity. To our knowledge, this is the first report of the use of ^{15}N isotopes to aid in the study of aqueous NO_x species reduction over supported Pd catalysts.
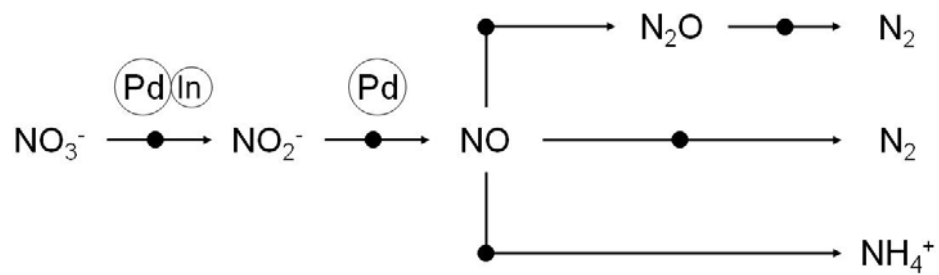
Scheme 1. Previous proposed nitrate reduction pathways

CHAPTER 2: EXPERIMENTAL

2.1 Reagents

Reagent grade sodium nitrite ($NaNO_2$) was purchased from Fisher. Sodium dihydrogen phosphate (H_2NaO_4P, 99.0%+) and sodium hydrogen phosphate ($HNa_2O_4P \cdot 2H_2O$, ~99%) were purchased from Fluka. ^{15}N-labeled sodium nitrite (^{15}N, 98%+), and gas cylinders of $^{15}N_2$ (98%+, for calibration) and ^{15}NO (^{15}N, 98%+) were purchased from Cambridge Isotope Laboratories (Andover, MA). Gas cylinders of ultrahigh purity hydrogen (H_2, 99.999%), nitrogen (N_2, 99.999%), nitric oxide (NO, 99.0%), and nitrous oxide (N_2O, 99.99%) were supplied by Matheson Tri-Gas (Joliet, IL). Deionized, nanopure water (DNW) was tap water purified by ion exchange (resistivity 16 M$\Omega \cdot$cm resistivity) and filtered through a nanopure membrane (Barnstead) to obtain a resistivity of 18 M$\Omega \cdot$cm. A 5 wt% Pd on γ-Al_2O_3 catalyst and Indium(III) nitrate hydrate ($In(NO_3)_3 \cdot xH_2O$, 99.999%) were purchased from Sigma-Aldrich.

2.2 Catalyst preparation and characterization

Pd/In catalysts were prepared by incipient wetness using a procedure described previously [41]. The nominal 5 wt% Pd on γ-Al_2O_3 catalyst was wet sieved to obtain particles <38 μm in diameter. Indium was then immobilized by pore volume impregnation of an $In(NO_3^-)_3$ solution. The Pd/In-γ-Al_2O_3 catalysts were then dried in air at 120 °C for 14 h and reduced with H_2 at 120 °C for 1 h. The catalyst had a final metal loading of 5.42wt%Pd and 0.86wt%In, as determined by ICP-MS (ELAN DRCe, Perkin Elmer SCIEX, CT), and a BET specific surface area of 104 m^2/g (ASAP 2020, Micromeritics).

2.3 Reduction experiments

A complete list of batch experiments performed is provided in **Table 1**. All catalytic

reduction experiments were performed at room temperature (21 ± 0.7 °C) in 120 ml glass serum bottles sealed with thick rubber stoppers, and were magnetically stirred at ca. 850 rpm to overcome external mass transfer limitations of $H_{2(aq)}$ to the catalyst surface. Each serum bottle was initially filled with 80 ml of DNW and phosphate buffer (pH 7, 20 mM), and then a desired amount of catalyst was introduced before sealing to form a closed system with 40 ml of headspace. The closed system was sparged with H_2 for 30 min while venting to reduce the Pd/In catalyst surface, remove dissolved oxygen, and saturate the solution and headspace with H_2. The target nitrogen species (NO_2^-, NO, or N_2O) was then added to the reactor alone or in combination with another nitrogen species to initiate reaction. Headspace samples (0.1 mL) were then periodically collected and immediately analyzed by gas chromatography with mass spectrometry (GC-MS). Aqueous aliquots (1 mL) were also collected at regular intervals, filtered (0.45 μm PTFE; Cole-Parmer) to remove catalyst particles and quench reactions, and stored in a refrigerator at 4 °C before analysis.

Mass Balance Experiments. Labeled and unlabeled nitrite reduction experiments (Exps. 1 and 2) were carried out under the same conditions, with a catalyst concentration of 0.375 g/L and an initial NO_2^- concentration of 1 mM. Nitrogen mass balances for the two cases were calculated for the whole reactor (aqueous and gas phase) using aqueous concentrations of NO_2^- and NH_4^+ and headspace gas concentrations of N_2, N_2O, and NO. We assumed that headspace gases were in equilibrium with aqueous phase concentrations of the same species at all times (i.e., that aqueous/gas partitioning processes are rapid compared to the catalytic reaction). Excellent mass balances using labeled N species supports this assumption.

An unlabeled N_2O reduction experiment (Exp. 3) was carried out with a catalyst concentration of 0.25 g/L and 1 ml of N_2O at 1 atm. Samples from the aqueous phase and headspace were analyzed to determine intermediates and end-products. A ^{15}N-labeled NO reduction experiment (Exp. 7) was carried out with a catalyst

concentration of 0.375 g/L and 1 ml of $^{15}NO_{(g)}$ at 1 atm. Samples from the aqueous phase and headspace were analyzed to determine possible intermediates and end products.

Isotope Mixing Experiments. A series of ^{15}N-labeled nitrite and unlabeled nitrogen species ($^{14}N_2O$ or ^{14}NO) combined reduction experiments (Exps. 4, 5, and 6, with $^{14}N_2O$; Exps. 8, 9, and 10, with ^{14}NO) were carried out to assess the involvement of individual N species in N-N pairing reactions critical to N_2 formation. Each experiment was performed in triplicate. In each closed reactor system, a constant amount of $^{15}NO_2^-$ was added at time zero with varying amounts of $^{14}N_2O$ or ^{14}NO (yielding different $^{15}N{:}^{14}N$ ratios: 4:1, 1:1, 1:4, respectively). The purpose of varying the amounts of exogenous supplied unlabeled $^{14}N_2O/^{14}NO$ was to investigate its possible reaction with intermediates from $^{15}NO_2^-$ reduction, and to assess N_2O's and NO's impact on the selectivity for N_2 over NH_4^+ respectively. The final product distribution was determined for each reactor system when the component amounts in both aqueous and gaseous phases became constant.

Product Distribution Experiments. A series of reactions were conducted to measure the end-product distributions as a function of varying initial concentration of either ^{15}NO or $^{15}NO_2^-$ (Exps. 11-20, each triplicated). Each reactor was prepared and buffered in the same manner described above. After allowing reactions to reach completion, $^{15}N_2$ headspace and NH_4^+ aqueous concentrations were analyzed.

2.4 Analytical methods

All gas samples with N_2O, NO, and N_2 were analyzed by gas chromatography with mass spectrometry (GC-MS; Agilent Technologies, 6850 Network GC System, and 5975C VL MSD with Triple-Axis Detector; Column, Varian Plot CP-Molesieve 5Å, 25 m length × 0.25 mm i.d.; oven temperature 165 °C; helium as carrier gas, 1.0 ml/min). Mixed calibration standards were prepared in the same way as the reactor

setup: 120 ml serum bottle filled with 80 ml of DNW and phosphate buffer (pH 7, 20 mM), sealed with thick rubber stopper, sparged with H_2 for 30 min while venting. For one designated calibration standard, each gaseous nitrogen species ($^{14}N_2$, $^{15}N_2$, $^{14}N_2O$, ^{14}NO and ^{15}NO) was added into the closed system in the same volume at 1 atm. Similar GC-MS sensitivities were observed for ^{14}NO and ^{15}NO, but atmospheric interference of $^{14}N_2$ measurements prevented accurate comparison of MS detector sensitivity towards $^{15}N_2$.

Aqueous NO_3^- and NO_2^- concentrations were analyzed by ion chromatography with conductivity detection (Dionex ICS-2000 system; Dionex IonPac AS18 column; 36 mM KOH as eluent; 1 mL/min eluent flow rate; 25 μL injection loop). Ammonium concentrations were analyzed by UV-Vis colorimetric analysis (HACH DR/4000U spectrophotometry) using the low-range (0.02 to 2.50 mg/L NH_3-N) Test 'N Tube nitrogen ammonia reagent set from HACH.

Concentrations of all analytes are shown in terms of total moles of N in the closed reactor (i.e., aqueous + gas) so that all analytes can be represented on a common scale and to illustrate N mass balances that include contributions from monoatomic and diatomic N species. Product distributions are presented in terms of selectivity for the desired N_2 product, calculated using measurements of both N_2 and NH_4^+ according to Equation 1:

$$S_{N_2} = \frac{2n(N_2)}{2n(N_2) + n(NH_4^+)} \qquad \text{(Eq. 1)}$$

in which S_{N_2} is the selectivity for N_2; $n(N_2)$ and $n(NH_4^+)$ are the moles of N_2 and NH_4^+ monitored in actual reduction experiments respectively.

2.5 Tables

Table 1. List of experiments performed

Exp. No.	Catalyst loading (mg)	$^{15}NO_2^-$	NO_2^-	^{15}NO	NO	N_2O
		(mM)		(ml, at 1 atm)		
1	30		1			
2	30	1				
3	20					1
4*	10	1				0.25
5*	10	1				1
6*	10	1				4
7	30			1		
8*	10	1			0.5	
9*	10	1			2	
10*	10	1			8	
11*	30			0.1		
12*	30			0.2		
13*	30			0.5		
14*	30			1		
15*	30			2		
16*	10	0.125				
17*	10	0.25				
18*	10	1				
19*	10	2				
20*	10	4				

* Each experiment was performed in triplicate.

CHAPTER 3: RESULTS AND DISCUSSION

3.1 Labeled N eliminates background N_2 interference

Results from the unlabeled nitrite reduction experiment (Exp. 1) are shown in **Fig. 1(a)**. A loss of $NO_2^-{}_{(aq)}$ was observed, while $N_{2(g)}$ was detected in the gas phase and $NH_4^+{}_{(aq)}$ was formed in the aqueous phase. There was also transient formation and disappearance of $N_2O_{(g)}$ in the system, whereas no $NO_{(g)}$ was detected in the headspace. The calculated total moles of N during the reaction (represented by the solid black line) increase with time, and markedly exceed the initial moles after 3 min of reaction (represented by the horizontal dashed line). This is attributed to atmospheric $N_{2(g)}$ (~210,000 ppm$_v$) leaking into the closed system during repeated sampling. The poor mass balance makes it challenging to quantify intermediates formed during the reduction process.

To avoid interference from atmospheric nitrogen, ^{15}N-labeled NO_2^- was used in the place of unlabeled NO_2^- for catalytic reduction under the same experimental conditions (Exp. 2). Results are shown in **Fig. 1(b)**. The observed pseudo-first-order rate constant for $^{15}NO_2^-{}_{(aq)}$ reduction (k_{obs} = 20.2 L/(min, g Pd)) and concentration of $NH_4^+{}_{(aq)}$ produced during the reaction (32 μmol) are similar to those observed with unlabeled NO_2^- (k_{obs} = 18.9 L/(min, g Pd); 27 μmol NH_4^+), indicating that kinetic isotope effects are not significant. Pseudo-first-order rate constants for NO_2^- reduction at pH 5.0 on 5wt% Pd/γ-Al_2O_3 and 5wt%Pd-0.5wt%In/γ-Al_2O_3 were 4.4 L/(min, g Pd) and 7.6 L/(min, g Pd) respectively, as reported by Shuai et al [15]. The difference in k_{obs} may be due to differing experimental conditions, e.g. pH, and catalyst loading. The total moles of nitrogen agree with the initial moles of nitrogen throughout the reaction after eliminating interference from atmospheric $^{14}N_2$. The labeled intermediate $^{15}N_2O$ was also detected during the reaction; however, no significant ^{15}NO was detected. A selectivity of 65.0% for N_2 was observed for $^{15}NO_2^-$ reduction, which was calculated using both measurements of N_2 and NH_4^+. Previously only

NH_4^+ produced from NO_2^- reduction was used to calculate selectivity, assuming the remaining fraction of the product mass balance was N_2 [29,42].

3.2 Confirmation of N$_2$O as an intermediate

Reduction experiments with N_2O as the initial reactant alone and in the presence of NO_2^- were performed in order to determine if N_2O is a key intermediate in determining product selectivity. When used alone, N_2O was unlabeled due to its excessive cost (~\$6000 per liter of $^{15}N_2O$). Results are shown in **Fig. 2(a)** for the case when $N_2O_{(g)}$ was the only initial reactant (Exp. 3). Only $N_{2(g)}$ was detected in the headspace, and no $NH_4^+{}_{(aq)}$ was detected in aqueous samples either during the reaction or at the end of the reaction, indicating that N_2O is only reduced to N_2, and has no contribution to NH_4^+ production. Mass balance results in **Fig. 2(a)** indicate leaking of background nitrogen into bottles was not a significant concern over the experimental time scale. This is because extracting only gas and not liquid samples reduces sampling time and frequency compared to NO_2^- reduction experiments.

Results are shown in **Fig. 2(b)** for reactions where unlabeled $N_2O_{(g)}$ is initially added to the reactor at the same time as ^{15}N-labeled NO_2^- (Exps. 4-6). No mixed-labeled $N_{2(g)}$ (MW: 29) was detected with increasing initial $N_2O_{(g)}$ concentrations, and the amounts of $^{15}N_{2(g)}$ (MW: 30) and $NH_4^+{}_{(aq)}$ production was unaffected by the amount of unlabeled N_2O initially added to the reactor at time zero. This indicates that N_2O reacts stoichiometrically to form N_2 and does not interact with either NO_2^- or any of its other reduction intermediates on the catalyst surface.

The N_2O results generally support the previously proposed mechanism (**Scheme 1**) that N_2 but not NH_4^+ is produced from N_2O reduction. The mass-normalized reduction rate constant (k_{obs}) for N_2O reduction is 13.1 L/(min, g Pd), smaller than that of NO_2^- reduction (k_{obs} = 20.2 L/(min, g Pd)). This enables detection of N_2O in the reactor headspace when monitoring NO_2^- reduction in this study (**Fig. 1**), as well as previous

studies reporting on reduction of NO_3^-, NO_2^-, and NO [32,35,37]. Sa et al [43] proposed that the formation of gaseous N_2O is related to the high surface coverage of NO_2^-. The presence of $N_2O_{(g)}$ in the gas phase during NO_2^- reduction in our work supports this assertion.

3.3 Confirmation of NO as an intermediate

Reduction experiments with NO as the initial reactant alone and in the presence of NO_2^- were performed in order to determine if NO affects selectivity. Results are shown in **Fig. 3(a)** for the case when ^{15}NO was the only initial reactant (Exp. 7). ^{15}N-labeled NO was used to maintain a mass balance, enabling correct measurement of N_2 produced from NO. $^{15}N_2O$ (MW: 46) was also detected in the headspace as an intermediate. The final product $^{15}N_2$ was detected in the headspace, and NH_4^+ was detected in the aqueous phase, indicating that NO reduction can lead to both end products, as well as N_2O. Since the mass-normalized reduction rate constant (k_{obs}) for NO reduction is 1.3 L/(min, g Pd), much smaller than those of NO_2^- and N_2O reduction (k_{obs} = 20.2 and 13.1 L/(min, g Pd), respectively), the accumulation of NO should be expected during NO_2^- reduction experiments, unless the adsorbed NO that forms on the catalyst surface from NO_2^- reduction is strongly bound and/or much more reactive than externally supplied NO.

Results are shown in **Fig. 3(b)** for the cases when unlabeled NO is initially added along with ^{15}N-labeled NO_2^- (Exps. 8-10). The production of mixed-labeled N_2 (MW: 29) increases with increasing initial concentrations of unlabeled NO. This indicates that NO is a reaction intermediate of NO_3^-. It also demonstrates that NO_2^- or one of its daughter intermediates/products interact with NO (or a daughter product thereof) to form N_2. Since no NO was detected in the headspace during NO_2^- reduction experiments, and mass balances are good, it is likely that the intermediate NO is in an adsorbed and highly reactive form on the catalyst surface. Ebbesen et al (2008) [34] reported infrared spectroscopic data that indicated the formation of NO_{ads} during NO_2^-

reduction on a supported Pd catalyst.

These NO results are consistent with **Scheme 1**, and contradict reports by Ebbesen et al [34] that no ammonium is formed from NO_{ads} during NO_2^- reduction on a Pd/Al_2O_3 catalyst. The fact that NO reduction can follow two parallel pathways, one leading to N_2 production and the other to NH_4^+ production, indicates that NO might be the key intermediate that controls the final product selectivity. Results from gas phase catalysis studies support this assertion. For example, Miller et al [37] observed N_2, N_2O, NH_3 during reduction of NO pulsed with H_2 over Pd/Al_2O_3 at 773 K. Hornung et al observed these same products during reduction of NO with H_2 on $Ru/\gamma-Al_2O_3$, and selectivity for N_2 reaching 100% at temperatures as low as 470 K [38]. This same author performed temperature-programmed surface reaction (TPSR) experiments and found that higher heating rates and lower H_2 partial pressures shift selectivity from NH_3 to N_2.

Van Hardeveld et al [39] studied NH_3 formation during NO_x reduction on a three-way Ru catalyst. They proposed that NO dissociates into adsorbed N and O atoms, and hydrogenation to NH_3 occurs stepwise by addition of H atoms to N_{ads} produced by NO dissociation. Several authors have also studied N_2O formation during NO reduction [44,45]. Results indicate that NO reduction to N_2O takes place via the formation of an NO dimer, $(NO)_2$, which results from weak adsorption of NO molecules on Pd sites [44,46]. This leads to N-N bond formation during the catalytic reduction of NO [47].

3.4 The effects of intermediate NO concentrations on selectivity for N_2 over NH_4^+.

The effect of NO concentration on selectivity is apparent in the isotope mixing experiments (**Fig. 3(b)**). With increasing unlabeled NO present in the system with $^{15}NO_2^-$, the production of total NH_4^+ decreased by up to 35% compared to the

$^{15}NO_2^-$-only batch reaction; recall that no effect on NH_4^+ occurred when $^{15}NO_2^-$ was reduced in the presence of excess unlabeled N_2O. This suggests that the concentration of NO may affect the N_2/NH_4^+ $_{(aq)}$ product selectivity. It has been generally accepted that the selectivity is a function of the ratio of the surface coverage of intermediate N-species to reductant species [24], and this key intermediate may be NO_{ads}. It is proposed that higher concentrations of NO intermediate would results in lower NH_4^+ production and higher selectivity for N_2. With higher NO concentrations on the catalyst surface, interactions between adsorbed N-O molecules increase, and at the same time, NO molecules have less exposure to Pd-adsorbed H atoms. Therefore, N_2 production from N-N coupling becomes more favored over NH_4^+ production, leading to an improved selectivity for N_2.

The effect of NO concentration on selectivity is further explored in **Fig. 4(a)**, where selectivity for N_2 is explored as a function of initial ^{15}NO concentration (Exps. 11-15). Increasing the initial amount of ^{15}NO increases the selectivity for N_2, reaching a maximum selectivity of ~0.9. However, when the initial NO concentration exceeds 20 μmol (13.3 μmol/mg Pd), no further increases in selectivity is observed. This is attributed to saturation of NO adsorption/reaction sites on the catalyst surface, and the plateau value of 20 μmol NO is on the same order as the calculation of the theoretical maximum NO coverage on 30 mg of a 5.42% Pd catalyst, *i.e.* 5.7 μmol NO_{ads} (or 3.8 μmol NO_{ads}/mg Pd). The NO coverage on Pd clusters was estimated by assuming the following: (1) spherical Pd nanoparticles; (2) Pd active sites are occupied by N atoms in NO_{ads} molecules; and (3) monolayer coverage of NO molecules on all surfaces of Pd clusters. The mean diameter (d) of one Pd nanoparticle in the catalyst is 3.12 nm, and $\rho_{Pd} = 1.2 \times 10^4 \, kg/m^3$. For one Pd cluster,

$$A_{surface} = 4\pi r^2 = \pi d^2$$

$$V = \frac{4}{3}\pi r^3 = \frac{1}{6}\pi d^3$$

$$m = \rho V = 1.91 \times 10^{-19} g$$

For 30 mg of a 5.42wt% Pd catalyst, the total mass of Pd is 1.626 mg. Thus, the number of Pd clusters and total surface of Pd sites in 30 mg catalyst can be determined as,

$$N_{Pd} = \frac{1.626mg}{1.91 \times 10^{-19}g} = 8.50 \times 10^{15}$$

$$A_{total} = N_{Pd}A_{surface} = 2.60 \times 10^{17}nm^2$$

The dominant bonding between Pd and NO involves covalent σ bonds [46], but no bonds are formed between adjacent NO molecules packed on the Pd surface. Therefore, the van der Waals radius of the N atom ($r_W = 155pm$) is adopted for calculation instead of the covalent radius ($r_{cov} = 71pm$). The total number of adsorbed N atoms saturated on Pd sites can be determined as,

$$N_{NO} = N_N = \frac{A_{total}}{\pi r_W^2}$$

Dividing this by Avogadro's number ($N_A = 6.02 \times 10^{23}mol^{-1}$) results in an estimated saturation surface concentration $n_{NO} = 5.7\mu mol$. Although this calculation should only be considered a rough estimate, the close match to the experimental observations of 20 μmol supports the role of NO-NO reactions being critical to production of diatomic N products.

We indirectly evaluate the effects of NO concentration on selectivity by varying the initial ^{15}N-labeled NO_2^- concentration (Exps. 16-20); results are shown in **Fig. 4(b)**. Increasing initial amounts of NO_2^- in the system also increases selectivity for the N_2. However, when the initial NO_2^- exceeds 160 μmol (320 μmol/mg Pd), the selectivity shows no further improvement. The plateau value for $N_{2(g)}$ selectivity occurs at higher initial NO_2^- concentrations than NO concentrations (16.8 μmol/mg Pd). Because of its high reactivity, we proposed that NO_{ads} formed during NO_2^- reduction cannot accumulate to concentrations as high as in exogenous supplied ^{15}NO reductions. So, higher concentrations of NO_2^- are needed to produce sufficient NO_{ads} for maximum

coverage of catalyst active sites. The same trend regarding the effect of initial nitrite concentration on end product selectivity was reported by Chinthaginjala and coworkers (2010) [29], though no plateau in selectivity was observed due to a lower NO_2^- concentration range examined. Similar results were reported by Katsounaros et al (2008) [48] during studies of electrochemical NO_3^- reduction at a tin electrode. Hence, it appears that surface saturation of NO_{ads} will also occur for NO_3^- reduction at sufficiently high initial concentrations.

3.5 Confirmed nitrate reduction mechanisms

A nitrate/nitrite reduction mechanism (**Scheme 1**) has been proposed in previous studies [49,50,51]. Typically, NO_3^- is hydrogenated by palladium-based bimetallic catalysts, while NO_2^- and further intermediates can be reduced with Pd catalyst. With H_2 as the reducing agent, NO_3^- is converted to N_2 as a desired product and NH_4^+ as by-product. In this typical reaction scheme, the role of NO reduction on N_2 and NH_4^+ formation was previously unclear due to lack of direct experimental evidence. The findings of our research confirm the involvement of NO in the nitrate/nitrite reduction pathways and its key role in affecting the end product distribution of N_2 and NH_4^+. Therefore, a slightly revised reaction scheme is proposed in **Scheme 2**.

NO_3^- is proposed to adsorb onto Pd-In bimetallic sites of the catalyst and be reduced to NO_2^- by hydrogen. The intermediate NO_2^- undergoes fast reduction on Pd monometallic sites, and is converted to the intermediate NO. The adsorbed NO is stepwise reduced by H_2 to NH_4^+ and H_2O respectively. Parallel with direct reduction of NO_{ads}, $(NO)_2$ dimers can also be formed on Pd surfaces, and this interaction leads to the formation of N-N bonds, producing N_2O, which is subsequently reduced to N_2. With higher NO_{ads} concentrations on the catalyst surface, the formation of $(NO)_2$ dimers is favored, and direct reduction of NO_{ads} is disadvantageous due to lack of adjacent H/H_2. Therefore, a higher selectivity for N_2 can be observed. The same mechanism applies to decreasing N_2 selectivity corresponding to decreasing NO_{ads}

concentration.
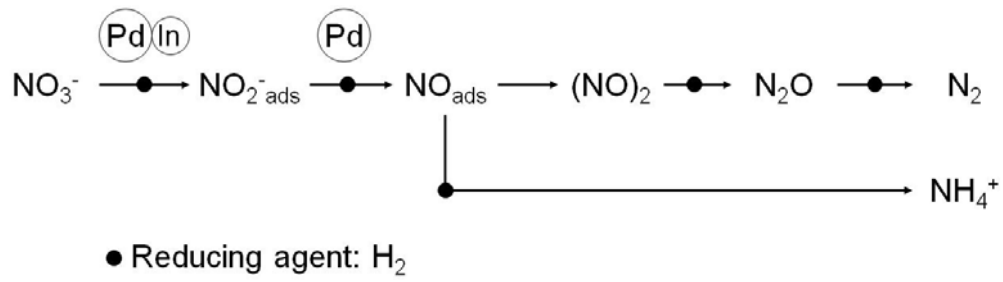
Scheme 2. Revised nitrate reduction pathways

3.6 Figures
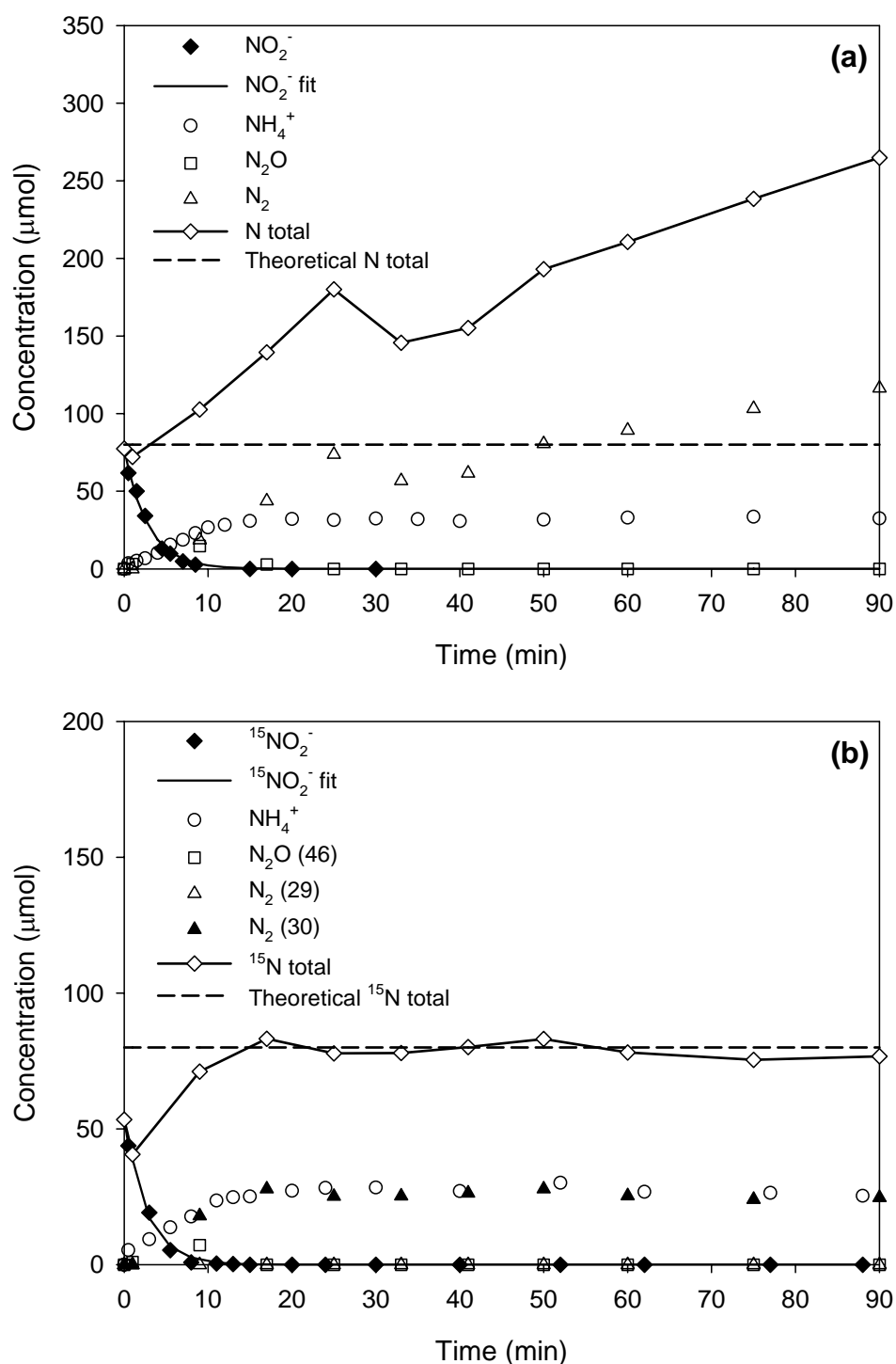
Figure 1. Nitrite reduction profiles (1 mM NO_2^-, 0.375 g/L catalyst) using (a) unlabeled NO_2^- and (b) $^{15}NO_2^-$. All analytes are plotted in terms of micromoles of molecules.
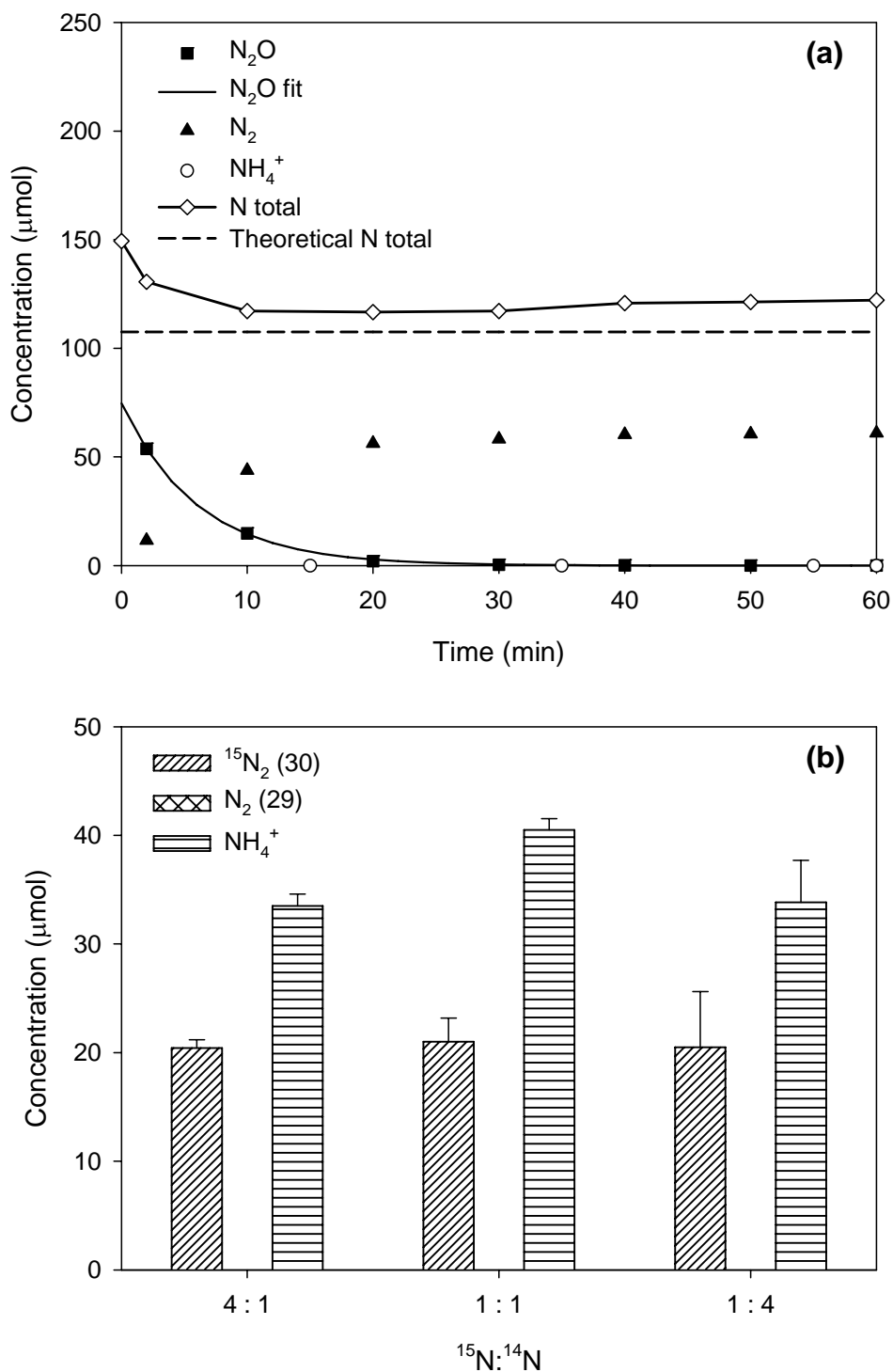
Figure 2. (a) N_2O reduction profiles (50 μmol N_2O, 0.25 g/L catalyst); (b) Final product distribution from the combined reduction of $^{15}NO_2^-$ (80 μmol) and different amounts of unlabeled N_2O (note that the values and error bars for N_2(29) are zeros).
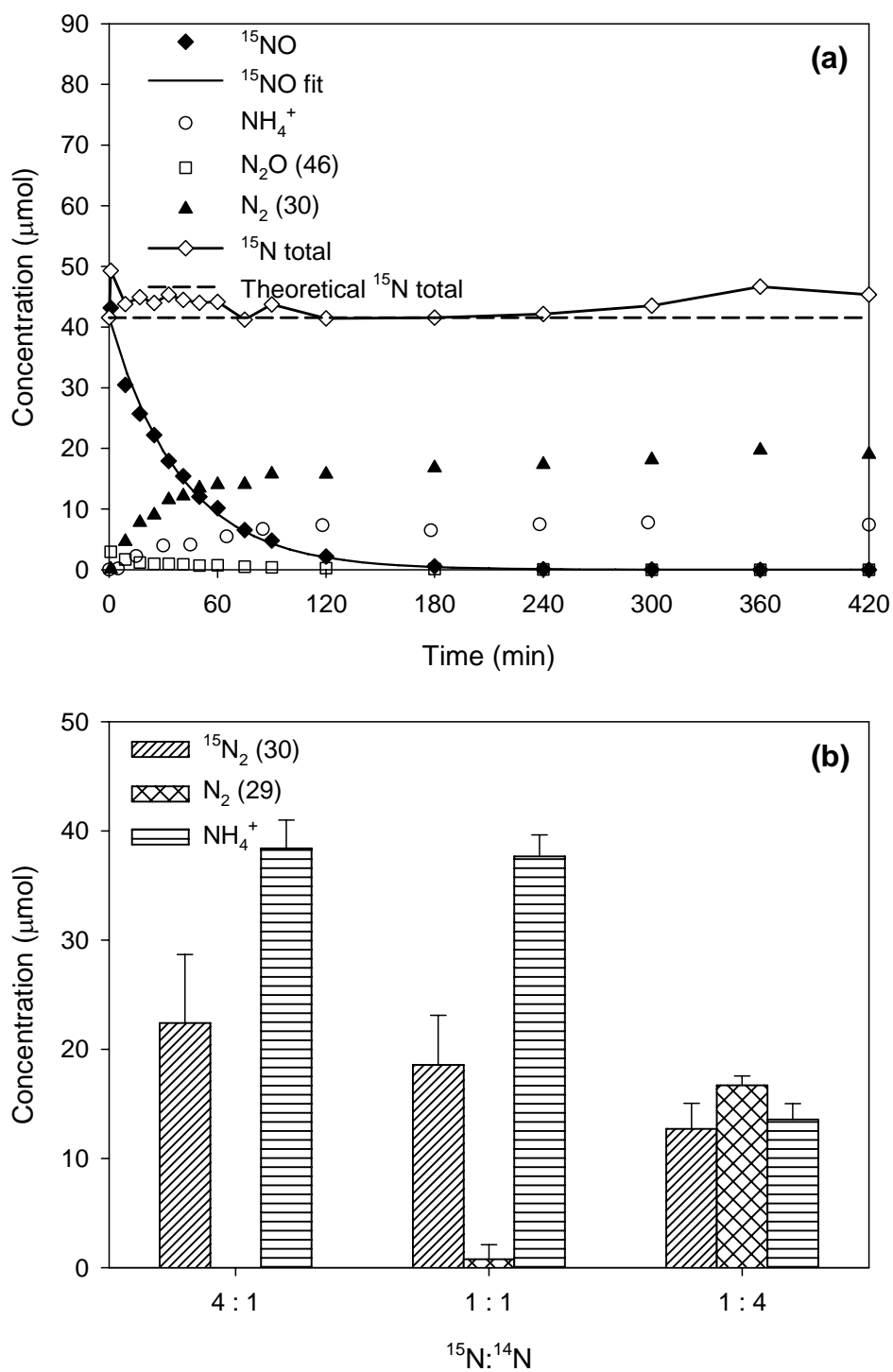
Figure 3. (a) ^{15}NO reduction profiles (41 μmol ^{15}NO, catalyst 0.375 g/L); (b) Final product distribution from the combined reduction of $^{15}NO_2^-$ (80 μmol) and different amounts of ^{14}NO.
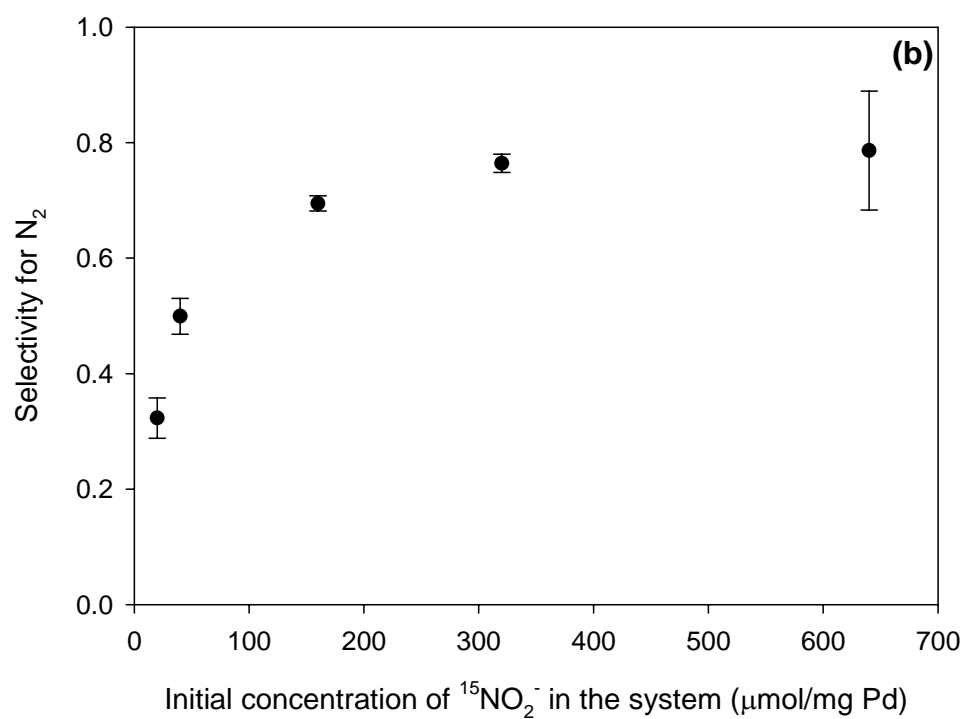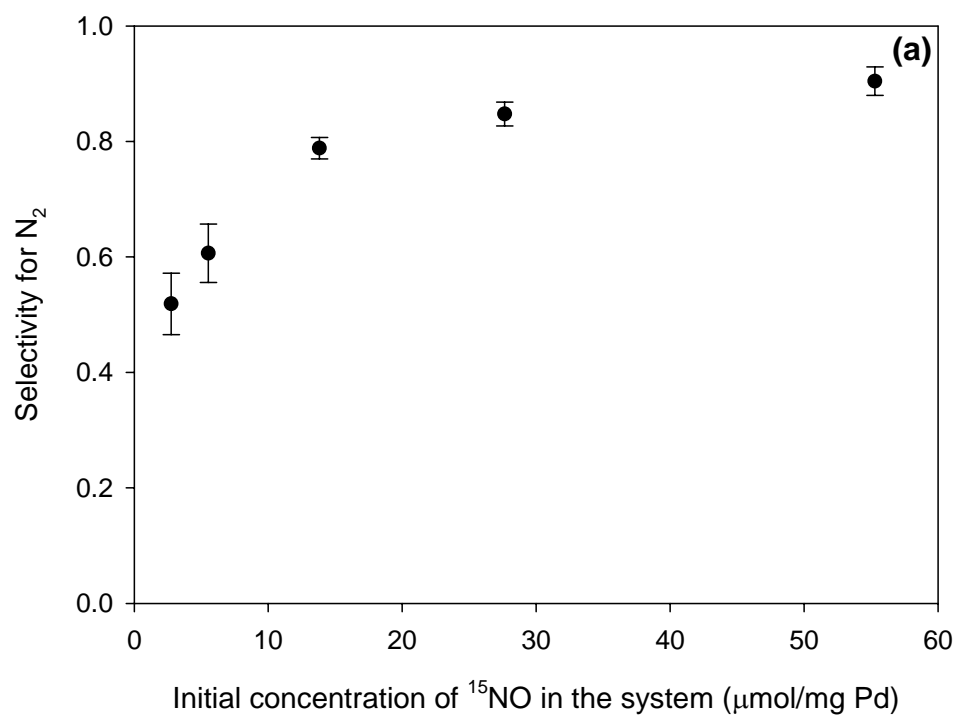
Figure 4. (a) Selectivity for N_2 with different initial amounts of NO; (b) Selectivity for N_2 with different initial amounts of $^{15}NO_2^-$.

CHAPTER 4: CONCLUSIONS

^{15}N-labeling was shown to be an effective tool for elucidation of the nitrate/nitrite reduction pathway by eliminating the effect of atmospheric $^{14}N_2$. For a Pd-In/Al_2O_3 catalyst, no isotope effect was observed for reaction kinetics. N_2O is confirmed as an intermediate in nitrate/nitrite reduction pathways; N_2O can only be reduced to N_2, and not NH_4^+. Using isotope mixing experiments, NO is confirmed as a key intermediate in nitrate/nitrite reduction pathway, and is responsible for both N_2 and NH_4^+ production. A highly reactive and strongly bound NO_{ads} species is formed on the catalyst surface, and no $NO_{(g)}$ is detected in the headspace. The $N_{2(g)}$/$NH_4^+{}_{(aq)}$ product selectivity is determined by NO_{ads} concentration. The selectivity for N_2 increases with increasing NO_{ads} concentrations on the catalyst surface, but cannot be further improved when NO_{ads} concentration reaches maximum surface coverage. A revised reaction scheme for catalytic hydrogenation of nitrate/nitrite has been proposed.

REFERENCES

[1] Wakida, F. T.; Lerner, D. N. Non-agricultural sources of groundwater nitrate: a review and case study. *Water Research*, 2005, 39, 3-16.

[2] Binns, H. J.; Forman, J. A.; Karr, C. J. *et al*. Drinking water from private wells and risks to children. *Pediatrics*, 2009, 123, 1599-1605.

[3] Cantor, K. P. Drinking water and cancer. *Cancer Causes and Control*, 1997, 8, 292-308.

[4] Puckett, L. J.; Tesoriero, A. J.; Dubrovsky, N. M. Nitrogen contamination of surficial aquifers – a growing legacy. *Environmental Science and Technology*, 2011, 45, 839-844.

[5] Kim, J.; Benjamin, M. M. Modeling a novel ion exchange process for arsenic and nitrate removal. *Water Research*, 2004, 38, 2053-2062.

[6] Yang, P. Y.; Nitisoravut, S.; Wu, J. S. Nitrate removal using a mixed-culture entrapped microbial cell immobilization process under high salt conditions. *Water Research*, 1995, 29, 1525-1532.

[7] Wisniewski, C.; Persin, F.; Cherif, T. et al. Denitrification of drinking water by the association of an electrodialysis process and a membrane bioreactor: feasibility and application. *Desalination*, 2001, 139, 199-205.

[8] Ersever, I.; Ravindran, V.; Pirbazari, M. Biological denitrification of reverse osmosis brine concentrates: II. Fluidized bed adsorber reactor studies. *Journal of Environmental Engineering and Science*, 2007, 6, 519-532.

[9] Aslan, S. Combined removal of pesticides and nitrates in drinking waters using biodenitrification and sand filter system. *Process Biochemistry*, 2005, 40, 417-424.

[10] Ergas, S. J.; Rheinheimer, D. E. Drinking water denitrification using a membrane bioreactor. *Water Research*, 2004, 38, 3225-3232.

[11] Moreno, B.; Gomez, M. A.; Gonzalez-Lopez, J.; Hontoria, E. Inoculation of a submerged filter for biological denitrification of nitrate polluted groundwater: a comparative study. *Journal of Hazardous Materials*, 2005, 117, 141-147.

[12] Soares, O. S. G. P.; Orfao, J. J. M.; Ruiz-Martinez, J. et al. Pd-Cu/AC and Pt-Cu/AC catalysts for nitrate reduction with hydrogen: Influence of calcinations and reduction temperatures. *Chemical Engineering Journal*, 2010, 165, 78-88.

[13] Mikami, I.; Kitayama, R.; Okuhara, T. Hydrogenations of nitrate and nitrite in water over Pt-promoted Ni catalysts. *Applied Catalysis A: General*, 2006, 297, 24-30.

[14] Chen, H.; Xu, Z.; Wan, H. et al. Aqueous bromate reduction by catalytic hydrogenation over Pd/Al_2O_3 catalysts. *Applied Catalysis B: Environmental*, 2010, 96, 307-313.

[15] Shuai, D.; Chaplin, B. P.; Shapley, J. R. et al. Enhancement of oxyanion and diatrizoate reduction kinetics using selected azo dyes on Pd-based catalysts. *Environmental Science and Technology*, 2010, 44, 1773-1779.

[16] Soares, O. S. G. P.; Orfao, J. J. M. Nitrate reduction catalyzed by Pd-Cu and Pt-Cu supported on different carbon materials. *Catalysis letters*, 2010, 139, 97-104.

[17] Chaplin, B. P.; Shapley, J. R. The selectivity and sustainability of a Pd-In/γ-Al$_2$O$_3$ catalyst in a packed-bed reactor: The effect of solution composition. *Catalysis Letters*, 2009, 130, 56-62.

[18] Palomares, A. E.; Franch, C.; Corma, A. Nitrate removal from polluted aquifers using (Sn or Cu)/Pd catalysts in a continuous reactor. *Catalysis Today*, 2010, 149, 348-351.

[19] Sa, J.; Vinek, H. Catalytic hydrogenation of nitrates in water over a bimetallic catalyst. *Applied Catalysis B: Environmental*, 2005, 57, 247-256.

[20] Berndt, H.; Monnich, I.; Lucke, B.; Menzel, M. Tin promoted palladium catalysts for nitrate removal from drinking water. *Applied Catalysis B: Environmental*, 2001, 30, 111-122.

[21] Soares, O. S. G. P.; Orfao, J. J. M.; Pereira, M. F. R. Activated carbon supported metal catalysts for nitrate and nitrite reduction in water. *Catalysis Letters*, 2008, 126, 253-260.

[22] Qi, G.; Yang, R. T.; Rinaldi, F. C. Selective catalytic reduction of nitric oxide with hydrogen over Pd-based catalysts. *Journal of Catalysis*, 2006, 237, 381-392.

[23] Pekridis, G.; Athanasiou, C.; Konsolakis, M. et al. N$_2$O abatement over γ–Al$_2$O$_3$ supported catalysts: Effect of reducing agent and active phase nature. *Topics in Catalysis*, 2009, 52, 1880-1887.

[24] Prusse, U.; Vorlop, K.-D. Supported bimetallic palladium catalysts for water-phase nitrate reduction. *Journal of Molecular Catalysis A: Chemical*, 2001, 173, 313-328.

[25] Lemaignen, L.; Tong, C.; Begon, V. et al. Catalytic denitrification of water with palladium-based catalysts supported on activated carbons. *Catalysis Today*, 2002, 75, 43-48.

[26] Matatov-Meytal, Y.; Barelko, V.; Yuranov, I. et al. Cloth catalysts for water denitrification II. Removal of nitrates using Pd-Cu supported on glass fibers. *Applied Catalysis B – Environmental*, 2001, 31, 233-240.

[27] Horold, S.; Tacke, T.; Vorlop, K.-D. Catalytical removal of nitrate and nitrite from drinking water: 1. Screening for hydrogenation catalysis and influence of reaction conditions on activity and selectivity. *Environmental Technology*, 1993, 14, 931-939.

[28] Zhang, F.; Miao, S.; Yang, Y. et al. Size-dependent hydrogenation selectivity of nitrate on Pd-Cu/TiO2 catalysts. *Journal of Physical Chemistry C*, 2008, 112, 7665-7671.

[29] Chinthaginjala, J. K.; Lefferts, L. Support effect on selectivity of nitrite reduction in water. *Applied Catalysis B: Environmental*, 2010, 101, 144-149.

[30] Yoshinaga, Y.; Akita, T.; Mikami, I.; Okuhara, T. Hydrogenation of nitrite in water to nitrogen over Pd-Cu supported on active carbon. *Journal of Catalysis*, 2002,

207, 37-45.

[31] Chollier-Brym, M. J.; Gavagnin, R.; Strukul, G. *et al*. New insights in the solid state characteristics, in the possible intermediates and on the reactivity of Pd-Cu and Pd-Sn catalysts, used in denitrataion of drinking water. *Catalysis Today*, 2002, 75, 49-55.

[32] Nakamura, K.; Yoshida, Y.; Mikami, I.; Okuhara, T. Selective hydrogenation of nitrate in water over Cu-Pd/mordenite. *Applied Catalysis B: Environmental*, 2006, 65, 31-36.

[33] Witonska, I.; Karski, S.; Goluchowska, J. Kinetic studies on the hydrogenation of nitrate in water using Rh/Al_2O_3 and $Rh-Cu/Al_2O_3$ catalysts. *Kinetics and Catalysis*, 2007, 48, 823-828.

[34] Ebbesen, S. D.; Mojet, B. L.; Lefferts, L. *In situ* ATR-IR study of nitrite hydrogenation over Pd/Al_2O_3. *Journal of Catalysis*, 2008, 256, 15-23.

[35] Ebbesen, S. D.; Mojet, B. L.; Lefferts, L. Mechanistic investigation of the heterogeneous hydrogenation of nitrite over Pt/Al_2O_3 by attenuated total reflection infrared spectroscopy. *Journal of Physical Chemistry C*, 2009, 113, 2503-2511.

[36] Warna, J.; Turunen, I.; Salmi, T.; Maunula, T. Kinetics of nitrate reduction in monolith reactor. *Chemical Engineering Science*, 1994, 49, 5763-5773.

[37] Miller, D. D.; Chuang, S. S. C. Pulse transient responses of NO decomposition and reduction with H_2 on $Ag-Pd/Al_2O_3$. *Journal of Physical Chemistry C*, 2009, 113, 14963-14971.

[38] Hornung, A.; Muhler, M.; Ertl, G. On the mechanism of the selective catalytic reduction of NO to N_2 by H_2 over Ru/MgO and Ru/Al_2O_3 catalysts. *Topics in Catalysis*, 2000, 11, 263-270.

[39] Van Hardeveld, R. M.; Van Santen, R. A.; Niemantsverdriet, J.W. Formation of NH_3 and N_2 from atomic nitrogen and hydrogen on rhodium (111). *Journal of Vacuum Science and Technology A – Vacuum Surfaces and Films*, 1997, 15, 1558-1562.

[40] Chaplin, B. P.; Roundy, E.; Guy, K. A. et al. Effects of natural water ions and humic acid on catalytic nitrate reduction kinetics using an alumina supported Pd-Cu catalyst. *Environmental Science and Technology*, 2006, 40, 3075-3081.

[41] Chaplin, B. P.; Shapley, J. R.; Werth, C. J. Regeration of sulfur-fouled bimetallic Pd-based catalysts. *Environmental Science and Technology*, 2007, 41, 5491-5497.

[42] Marchesini, F. A.; Gutierrez, L. B.; Querini, C. A.; Miro, E. E. Pt, In and Pd, In catalysts for the hydrogenation of nitrates and nitrites in water. FTIR characterization and reaction studies. *Chemical Engineering Journal*, 2010, 159, 203-211.

[43] Sa, J.; Anderson, J. A. FTIR study of aqueous nitrate reduction over Pd/TiO_2. *Applied Catalysis B: Environmental*, 2008, 77,409-417.

[44] De Vooys, A. C. A.; Koper, M. T. M.; Van Santen, R. A.; Van Veen, J. A. R. Mechanistic study on the electrocatalytic reduction of nitric oxide on transition-metal electrodes. *Journal of Catalysis*, 2001, 202, 387-394.

[45] Burch, R.; Daniells, S. T.; Hu, P. The mechanism of N_2O formation via the $(NO)_2$

dimer: A density functional theory study. *Journal of Chemical Physics*, 2004, 121, 2737-2745.

[46] Smith, G. W.; Carter, E. A. Interactions of NO and CO with Pd and Pt atoms. *Journal of Physical Chemistry*, 1991, 95, 2327-2339.

[47] Brown, W. A. NO chemisorptions and reactions on metal surfaces: A new perspective. *Journal of Physical Chemistry B*, 2000, 104, 2578-2595.

[48] Katsounaros, I.; Kyriacou, G. Influence of nitrate concentration on its electrochemical reduciont on tin cathode: Identification of reaction intermediates. *Electrochimica Acta*, 2008, 53, 5477-5484.

[49] Pintar, A.; Batista, J.; Levec, J.; Kajiuchi, T. Kinetics of the catalytic liquid-phase hydrogenation of aqueous nitrate solutions. *Applied Catalysis B: Environmental*, 1996, 11, 81-98.

[50] Daub, K.; Emig, G.; Chollier, M.-J. et al. Studies on the use of catalytic membranes for reduction of nitrate in drinking water. *Chemical Engineering Science*, 1999, 54, 1577-1582.

[51] Prusse, U.; Hahnlein, M.; Daum, J.; Vorlop, K.-D. Improving the catalytic nitrate reduction. *Catalysis Today*, 2000, 55, 79-90.

APPENDIX: DATA USED FOR FIGURES

Data for Fig. 1(a) Unlabeled NO_2^- reduction profiles (1 mM NO_2^-, 0.375 g/L catalyst)

Table 2. Aqueous phase data for 1 mM $^{14}NO_2^-$ reduction

Time	NO_2^-	Time	NO_2^- fit	NH_4^+
(min)	(μmol)	(min)	(μmol)	
0.5	61.8	0.0	77.5	0.0
1.5	50.1	0.5	64.9	3.6
2.5	34.1	1.5	45.5	5.2
4.5	13.1	2.5	32.0	6.8
5.5	9.8	4.0	18.8	10.3
7.0	4.8	5.5	11.0	15.5
8.5	2.7	7.0	6.5	18.6
15.0	0.0	8.5	3.8	22.9
20.0	0.0	10.0	2.2	26.7
30.0	0.0	12.0	1.1	28.3
		15.0	0.4	30.9
		20.0	0.1	32.1
		25.0	0.0	31.4
		30.0	0.0	32.4
		35.0	0.0	32.0
		40.0	0.0	30.7
		50.0	0.0	31.7
		60.0	0.0	33.0
		75.0	0.0	33.5
		90.0	0.0	32.5

Table 3. Gaseous phase data for 1 mM $^{14}NO_2^-$ reduction

Time	N_2O (44)	N_2 (28)	N total	Theoretical N total
(min)		(μmol)		
0.0	0.0	0.0	77.4	80.0
1.0	3.1	0.0	72.1	80.0
9.0	14.7	18.7	102.7	80.0
17.0	2.9	43.7	139.5	80.0
25.0	0.0	73.7	180.0	80.0
33.0	0.0	56.8	145.7	80.0
41.0	0.0	61.6	155.2	80.0
50.0	0.0	80.5	193.1	80.0
60.0	0.0	89.3	210.7	80.0
75.0	0.0	103.2	238.4	80.0
90.0	0.0	116.4	264.8	80.0

Species N_2O (45, 46) and N_2 (29, 30) were also monitored but not detected or below the detection limit of 0.1 μmol.

Data for Fig. 1(b) $^{15}NO_2^-$ reduction profiles (1 mM $^{15}NO_2^-$, 0.375 g/L catalyst)

Table 4. Aqueous phase data for 1 mM $^{15}NO_2^-$ reduction

Time	$^{15}NO_2^-$	Time	$^{15}NO_2^-$ fit	NH_4^+
(min)	(μmol)	(min)	(μmol)	
0.5	43.8	0.0	53.4	0.0
3.0	19.1	0.5	44.2	5.3
5.5	5.3	3.0	17.2	9.3
8.0	0.8	5.5	6.7	13.7
11.0	0.4	8.0	2.6	17.7
13.0	0.2	11.0	0.8	23.6
15.0	0.0	13.0	0.4	24.8
20.0	0.0	15.0	0.2	25.0
24.0	0.0	20.0	0.0	27.2
30.0	0.0	24.0	0.0	28.2
40.0	0.0	30.0	0.0	28.4
52.0	0.0	40.0	0.0	27.0
62.0	0.0	52.0	0.0	30.1
77.0	0.0	62.0	0.0	26.8
88.0	0.0	77.0	0.0	26.4
		88.0	0.0	25.3

Table 5. Gaseous phase data for 1 mM $^{15}NO_2^-$ reduction

Time	N$_2$O (46)	N$_2$ (29)	N$_2$ (30)	^{15}N total	Theoretical ^{15}N total
(min)			(μmol)		
0.0	0.0	0.0	0.0	53.4	80.0
1.0	0.9	0.0	0.0	40.6	80.0
9.0	7.2	0.0	18.0	71.1	80.0
17.0	0.0	0.0	27.8	83.2	80.0
25.0	0.0	0.0	25.2	77.8	80.0
33.0	0.0	0.0	25.2	77.9	80.0
41.0	0.0	0.0	26.3	80.1	80.0
50.0	0.0	0.0	27.8	83.1	80.0
60.0	0.0	0.0	25.4	78.1	80.0
75.0	0.0	0.0	24.0	75.4	80.0
90.0	0.0	0.0	24.7	76.7	80.0

Species N$_2$O (44, 45) and N$_2$ (28) were also monitored but not listed. Amounts of N$_2$O (44, 45) were below the detection limit of 0.1 μmol, and N$_2$ (28) was twofold of measured N$_2$ (30).

Data for Fig. 2(a) N_2O reduction profiles (50 µmol N_2O, 0.25 g/L catalyst)

Table 6. Aqueous phase data for N_2O reduction

Time (min)	NH_4^+ (µmol)
15.0	0.0
35.0	0.0
55.0	0.0
60.0	0.0

Table 7. Gaseous phase data for N_2O reduction

Time	N_2O (44)	N_2 (28)	N total	Theoretical N total	Time	N_2O fit
(min)	(μmol)				(min)	(μmol)
0.0			149.3	107.5	0.0	74.7
2.0	53.7	11.6	130.6	107.5	2.0	53.8
10.0	14.8	43.8	117. 2	107.5	4.0	38.7
20.0	2.1	56.2	116.6	107.5	6.0	27.9
30.0	0.3	58.2	117.1	107.5	8.0	20.1
40.0	0.1	60.3	120.8	107.5	10.0	14.4
50.0	0.1	60.6	121.3	107.5	12.0	10.4
60.0	0.0	61.0	122.1	107.5	14.0	7.5
					16.0	5.4
					18.0	3.9
					20.0	2.8
					22.0	2.0
					24.0	1.4
					26.0	1.0
					28.0	0.7
					30.0	0.5
					32.0	0.4
					34.0	0.3
					36.0	0.2
					38.0	0.1
					40.0	0.1
					42.0	0.1
					44.0	0.1
					46.0	0.0
					48.0	0.0
					50.0	0.0
					60.0	0.0

Species N_2 (29, 30) were also monitored but not detected or below the detection limit of 0.1 μmol.

Data for Fig. 2(b) Final product distribution from the combined reduction of $^{15}NO_2^-$ (80 μmol) and different amounts of unlabeled N_2O

Table 8. Summary of $^{15}NO_2^-$ and N_2O combined reductions

$^{15}N:^{14}N$	Average			Standard Deviation		
	N_2 (30)	N_2 (29)	NH_4^+	N_2 (30)	N_2 (29)	NH_4^+
	(μmol)					
4:1	20.4	0.0	33.5	0.8	0.0	1.1
1:1	21.0	0.0	40.5	2.2	0.0	1.0
1:4	20.5	0.0	33.8	5.1	0.0	3.9

Table 9. Replicates of $^{15}NO_2^-$ and N_2O combined reductions

$^{15}N:^{14}N$	Product	Replicate 1	Replicate 2	Replicate 3	Average	Standard Deviation
		(μmol)				
4:1	N_2 (30)	21.3	19.9	20.1	20.4	0.8
	N_2 (29)	0.0	0.0	0.0	0.0	0.0
	NH_4^+	34.6	32.4	33.5	33.5	1.1
1:1	N_2 (30)	18.5	22.0	22.5	21.0	2.2
	N_2 (29)	0.0	0.0	0.0	0.0	0.0
	NH_4^+	41.7	39.8	40.0	40.5	1.0
1:4	N_2 (30)	15.1	25.3	21.1	20.5	5.1
	N_2 (29)	0.0	0.0	0.0	0.0	0.0
	NH_4^+	29.7	37.4	34.4	33.8	3.9

Data for Fig. 3(a) [15]NO reduction profiles (41 μmol [15]NO, catalyst 0.375 g/L)

Table 10. Aqueous phase data for [15]NO reduction

Time	NH_4^+
(min)	(μmol)
0.0	0.0
5.0	0.2
15.0	2.2
30.0	4.0
45.0	4.1
65.0	5.5
85.0	6.7
118.0	7.3
178.0	6.5
238.0	7.5
298.0	7.7
420.0	7.4

Table 11. Gaseous phase data for ^{15}NO reduction

Time	^{15}NO	N$_2$O (46)	N$_2$ (30)	^{15}N total	Theoretical ^{15}N total	Time	^{15}NO fit
(min)			(μmol)			(min)	(μmol)
0.0				41.6	41.6	0.0	41.6
1.0	43.2	2.9	0.1	49.3	41.6	10.0	32.3
9.0	30.4	1.7	4.7	43.8	41.6	20.0	25.1
17.0	25.7	1.2	7.8	45.0	41.6	30.0	19.5
25.0	22.2	1.0	9.0	44.0	41.6	40.0	15.2
33.0	17.9	1.0	11.5	45.3	41.6	50.0	11.8
41.0	15.4	0.9	12.1	44.5	41.6	60.0	9.1
50.0	12.0	0.7	13.5	44.0	41.6	70.0	7.1
60.0	10.1	0.7	14.0	44.1	41.6	80.0	5.5
75.0	6.5	0.5	14.1	41.2	41.6	90.0	4.3
90.0	4.8	0.4	15.7	43.7	41.6	100.0	3.3
120.0	2.2	0.3	15.7	41.4	41.6	110.0	2.6
180.0	0.5	0.1	16.8	41.6	41.6	120.0	2.0
240.0	0.1	0.0	17.4	42.1	41.6	130.0	1.6
300.0	0.0	0.0	18.1	43.5	41.6	140.0	1.2
360.0	0.0	0.0	19.7	46.7	41.6	150.0	0.9
420.0	0.0	0.0	19.0	45.3	41.6	160.0	0.7
						170.0	0.6
						180.0	0.4
						190.0	0.3
						200.0	0.3
						210.0	0.2
						220.0	0.2
						230.0	0.1
						240.0	0.1
						250.0	0.1
						260.0	0.1
						270.0	0.0
						280.0	0.0
						290.0	0.0
						300.0	0.0
						330.0	0.0
						360.0	0.0
						390.0	0.0
						420.0	0.0

Species N$_2$O (44, 45) and N$_2$ (28, 29) were also monitored but not listed. Amounts of N$_2$O (44, 45) and N$_2$ (29) were below the detection limit of 0.1 μmol, and N$_2$ (28) was twofold of measured N$_2$ (30).

Data for Fig. 3(b) Final product distribution from the combined reduction of $^{15}NO_2^-$ (80 μmol) and different amounts of ^{14}NO

Table 12. Summary of $^{15}NO_2^-$ and NO combined reductions

$^{15}N:^{14}N$	Average			Standard Deviation		
	N_2 (30)	N_2 (29)	NH_4^+	N_2 (30)	N_2 (29)	NH_4^+
			(μmol)			
4:1	22.4	0.0	38.4	6.3	0.0	2.6
1:1	18.6	0.8	37.7	4.6	1.3	2.0
1:4	12.8	16.8	13.8	3.3	1.2	2.0

Table 13. Replicates of $^{15}NO_2^-$ and NO combined reductions

$^{15}N:^{14}N$	Product	Rep. 1	Rep. 2	Rep. 3	Average	Standard Deviation
				(μmol)		
	N_2 (30)	24.7	15.3	27.2	22.4	6.3
4:1	N_2 (29)	0.0	0.0	0.0	0.0	0.0
	NH_4^+	38.9	35.6	40.7	38.4	2.6
	N_2 (30)	23.8	16.4	15.5	18.6	4.6
1:1	N_2 (29)	0.0	0.0	2.3	0.8	1.3
	NH_4^+	36.9	39.9	36.2	37.7	2.0
	N_2 (30)	15.1	10.4	12.6	12.7	2.4
1:4	N_2 (29)	17.6	15.9	16.6	16.7	0.9
	NH_4^+	15.2	12.4	13.1	13.6	1.5

Data for Fig. 4(a) Selectivity for N_2 with different initial amounts of NO

Table 14. Summary of selectivity for N_2 with different initial amounts of NO

^{15}NO injected (ml, 1 atm)	^{15}NO C_0 (μmol/mg Pd)	Selectivity for N_2				
		Rep. 1	Rep. 2	Rep. 3	Average	Standard Deviation
0.1	2.8	0.5	0.5	0.6	0.5	0.1
0.2	5.5	0.6	0.6	0.6	0.6	0.1
0.5	13.8	0.8	0.8	0.8	0.8	0.0
1.0	27.6	0.8	0.8	0.9	0.8	0.0
2.0	55.3	0.9	0.9	0.9	0.9	0.0

Table 15. Replicates of selectivity for N_2 with different initial amounts of NO

^{15}NO injected (ml, 1 atm)	Product (μmol)	Rep. 1	Rep. 2	Rep. 3	Average	Standard Deviation
0.1	N_2 (30)	1.4	1.4	2.1		
	NH_4^+	3.0	2.8	3.0		
	selectivity	0.5	0.5	0.6	0.5	0.1
0.2	N_2 (30)	3.4	3.0	2.9		
	NH_4^+	3.7	3.7	4.8		
	selectivity	0.6	0.6	0.6	0.6	0.1
0.5	N_2 (30)	9.2	9.2	9.5		
	NH_4^+	4.5	5.6	4.9		
	selectivity	0.8	0.8	0.8	0.8	0.0
1.0	N_2 (30)	20.8	18.5	21.6		
	NH_4^+	8.2	7.3	6.4		
	selectivity	0.8	0.8	0.9	0.8	0.0
2.0	N_2 (30)	38.9	42.0	58.6		
	NH_4^+	10.8	8.6	9.2		
	selectivity	0.9	0.9	0.9	0.9	0.0

Data for Fig. 4(b) Selectivity for N_2 with different initial amounts of $^{15}NO_2^-$

Table 16. Summary of selectivity for N_2 with different initial amounts of $^{15}NO_2^-$

$^{15}NO_2^-$ C_0		Selectivity for N_2				
(mM)	(µmol/mg Pd)	Rep. 1	Rep. 2	Rep. 3	Average	Standard Deviation
0.125	20.0	0.3	0.4	0.3	0.3	0.0
0.25	40.0	0.5	0.5	0.5	0.5	0.0
1.0	160.0	0.7	0.7	0.7	0.7	0.0
2.0	320.0	0.8	0.8	0.7	0.8	0.0
4.0	640.0	0.7	0.8	0.8	0.8	0.1

Table 17. Replicates of selectivity for N_2 with different initial amounts of $^{15}NO_2^-$

$^{15}NO_2^-$ C_0 (mM)	Product (µmol)	Rep. 1	Rep. 2	Rep. 3	Average	Standard Deviation
0.125	N_2 (30)	2.0	1.9	1.6		
	NH_4^+	9.8	6.8	6.7		
	selectivity	0.3	0.4	0.3	0.3	0.0
0.25	N_2 (30)	5.3	5.7	5.1		
	NH_4^+	10.4	10.2	11.7		
	selectivity	0.5	0.5	0.5	0.5	0.0
1.0	N_2 (30)	28.1	32.2	30.4		
	NH_4^+	24.2	26.9	28.6		
	selectivity	0.7	0.7	0.7	0.7	0.0
2.0	N_2 (30)	65.6	68.0	63.2		
	NH_4^+	40.4	38.4	42.5		
	selectivity	0.8	0.8	0.7	0.8	0.0
4.0	N_2 (30)	84.7	132.0	126.5		
	NH_4^+	84.4	48.2	46.1		
	selectivity	0.7	0.8	0.8	0.8	0.1